Postharvest Biology and Technology 211 (2024) 112802

Contents lists available at ScienceDirect

Postharvest Biology and Technology

journal homepage: www.elsevier.com/locate/postharvbio

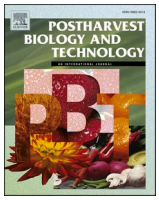

Detecting internal browning in apple tissue as determined by a single CT slice in intact fruit

Rachael M. Wood [a,*], Dirk E. Schut [b], Anna K. Trull [c], Leo F.M. Marcelis [a], Rob E. Schouten [d]

[a] Horticulture and Product Physiology, Wageningen University and Research, Droevendaalsesteeg 1, 6708 PB Wageningen, the Netherlands
[b] Computational Imaging, Centrum Wiskunde en Informatica (CWI), Science Park 123, 1098 XG Amsterdam, the Netherlands
[c] Greefa Machinebouw B. V, Langstraat 12, 4196 JB Tricht, the Netherlands
[d] Wageningen Food and Biobased Research, Bornse Weilanden 9, 6708 WG Wageningen, the Netherlands

ARTICLE INFO

Keywords:
Cavities
Controlled atmosphere
Fruit quality
Non-destructive
Postharvest
Physiological disorders

ABSTRACT

Internal browning (IB) in apples is associated with small voids that appear dark in X-ray computed tomography (CT) scans. Previous reports investigating IB in apples have used high resolution CT. However, for high-throughput in-line sorting and grading, detection of IB using CT, the image resolution and number of CT slices analysed must be limited. This work aimed to determine if IB can be accurately detected using a single CT slice with an image resolution that is not high enough to detect individual cells and pores in whole 'Kanzi' and 'Braeburn' fruit. Whole 'Kanzi' fruit (n = 120), previously stored under controlled atmosphere conditions (4 °C, 1 kPa O_2, 1.5 kPa CO_2) for eight months, were scanned with CT at a voxel size of approximately 130 μm. Whole 'Braeburn' fruit (n = 79) were stored under browning inducing conditions (0.5 °C, 1.5 kPa O_2, 5 kPa CO_2) for 2 and 3 months before scanning. For both cultivars, fruit ('Kanzi' = 20, 'Braeburn' = 38) that were stored under regular air conditions for one month were included as a non IB control. Following scanning, fruit were visually scored on browning intensity and type. An image-processing procedure based on grey-level threshold values was developed to determine the area percentage of detectable voids in CT slices. For both cultivars, the void percentage (V_p) in CT slices increased as the browning intensity in apple flesh increased. The largest variation in V_p among browning intensity classes was within the first 20 mm from the fruit stem end for 'Kanzi' fruit and between 30 and 40 mm for 'Braeburn' fruit. These results were due to the high incidence of radial flesh browning (RFB) within 'Kanzi' samples, which occurred concurrently with core browning at equal intensity. For 'Braeburn' fruit, RFB occurred in fruit with severe core browning. Logistic regression modelling using the V_p of CT slices at 30 and 35 mm of the fruit stem end showed better performance [area under the receiver operating characteristic curve (AUC) > 0.9] for classifying affected 'Kanzi' and 'Braeburn' fruit than models using the whole fruit average. These results demonstrate that the entire fruit does not need to be analysed for accurate classification. Using only one slice per fruit for browning detection would greatly reduce image analysis time, which is imperative for in-line IB detection using CT.

1. Introduction

Internal browning (IB) is a physiological disorder that develops during controlled atmosphere (CA) storage, characterised by patches of brown flesh and cavities within fruit tissue. In addition, the regions of brown flesh are associated with off-flavour (Hatoum et al., 2014). Browning occurs from the breakdown of cellular integrity, resulting in phenolic compounds becoming oxidised by the enzyme polyphenol oxidase (PPO) (Nicolas et al., 1994; Vaughn and Duke, 1984). Brown flesh and off-flavour are undesired traits; thus, fruit with IB are rendered unacceptable in the market. Different patterns of IB occur in different regions of fruit tissue, which are influenced by different pre-and-post-harvest factors (Sidhu et al., 2023).

IB disorders can be categorised into three types of injuries, including chilling injury, internal CO_2 injury and senescent breakdown (Sidhu et al., 2023). Senescent breakdown affects the cortex and vascular tissues of the whole fruit and can cause discolouration of the peel (Meheriuk et al., 1994). Radial flesh browning (RFB) is a senescence related IB disorder that affects the vascular tissue close to the stem end while the cortex tissue remains unaffected (James and Jobling, 2009;

* Correspondence to: Droevendaalsesteeg 1, 6708 PB Wageningen, the Netherlands.
E-mail address: rachw512@gmail.com (R.M. Wood).

https://doi.org/10.1016/j.postharvbio.2024.112802
Received 25 August 2023; Received in revised form 19 January 2024; Accepted 22 January 2024
Available online 2 February 2024

Sidhu et al., 2023). In contrast, diffuse flesh browning (DFB), associated with chilling injury, affects the cortex of the whole fruit while the vascular tissue remains relatively unaffected (James and Jobling, 2009; Sidhu et al., 2023). Core browning (CB) is associated with low temperatures and high CO_2 levels during storage and affects the core tissue next to the carpels while the outer cortex remains healthy (Meheriuk et al., 1994; Sidhu et al., 2023). Large fruit sizes, delayed harvests and light crop loads increase incidences of senescent breakdown, RFB, DFB and CB (Chigwaya et al., 2021a; Lee et al., 2013; Sidhu et al., 2023). Whereas warm temperatures before harvest increase RFB and DFB incidences but reduce CB (Sidhu et al., 2023). Fruit with IB do not exhibit any external symptoms, making in-line detection difficult. Detecting and removing affected fruit from the supply chain is crucial for reducing food wastage, as whole batches can be discarded despite a significant number of healthy fruit remaining in the batch (Van De Looverbosch et al., 2022). Therefore, an accurate method for detecting IB and other internal disorders is needed to maintain the commercial value of batches.

Most commercial grading symptoms that use visible and near-infrared (Vis-NIR) spectroscopy cannot reliably detect internal disorders (Huang et al., 2020; Nicolaï et al., 2014; Van De Looverbosch et al., 2020). In contrast, transmission Vis-NIR spectroscopy can detect IB with high levels of accuracy in research (Han et al., 2006; Huang et al., 2020; Khatiwada et al., 2016). However, the development of IB is not uniform; thus, multiple measurements from different positions are required for accurate predictions (Clark et al., 2003). Furthermore, large data sets over multiple seasons, from different locations for each cultivar, are needed for creating robust models using NIR (Peirs et al., 2002). Calibration models also depend on the spectrophotometer and cannot be easily transferred onto different devices, even from the same brand (Nicolaï et al., 2014).

Numerous studies have demonstrated that X-ray computed tomography (CT) can detect brown or damaged tissue in pome fruit (Diels et al., 2017; Herremans et al., 2013; Lammertyn et al., 2003; van Dael et al., 2019). CT combines multiple radiographs of the same fruit taken at different angles to generate a 3-dimensional volume of the fruit using a mathematical algorithm (Schut et al., 2022). The result is a 3D image with its voxels (3D pixels) representing X-ray energy attenuation, commonly viewed as a stack of 2D images coloured with a greyscale value (Janssen et al., 2020; van Dael et al., 2019). In CT scans, dark regions with low greyscale values correspond to regions of IB in affected fruit (Herremans et al., 2013; van Dael et al., 2019). The darker regions are due to the collapse of cell structures and the movement of water from affected tissue to healthy tissue, which causes the formation of cavities (Herremans et al., 2013). Air has a lower attenuation than water-rich fruit tissue; thus, intercellular air spaces or voids appear as dark regions in CT scans (Diels et al., 2017). CT has also been used to examine the porosity of different fruit and regions within fruit tissue (Chigwaya et al., 2021a; Janssen et al., 2020; Nugraha et al., 2019). Fruit porosity can be calculated from low-resolution scans by correlating the average greyscale values for a given region with actual porosity measured at high resolution (Chigwaya et al., 2021a; Janssen et al., 2020). Using Otsu's algorithm (Otsu, 1979), Diels et al. (2017) demonstrated that CT with a voxel size of 211 μm and image thresholding could detect and quantify bruise volumes in apples.

Prior reports assessing internal fruit damage with CT have used medical or laboratory scanners, which are expensive and time-consuming (Diels et al., 2017; Herremans et al., 2013; Lammertyn et al., 2003; van Dael et al., 2019). The largest voxel size in previous IB studies of apples using a laboratory CT scanner was 60 μm, which had a scan time of 30 min (Chigwaya et al., 2021b). Smaller voxel sizes require more X-ray images to reconstruct volumes accurately (Crowther et al., 1970), increasing exposure and acquisition time (Buzug, 2008). Furthermore, the large data size of 3D CT volumes can lead to long data processing times. Kotwaliwale et al. (2014) suggested that using one 2D CT slice at a predetermined location has a greater potential for practical applications than whole-fruit scans. A low acquisition and data processing time is crucial for high-throughput in-line detection of internal disorders using CT, which is related cubically to the resolution. However, smaller pores are not detected by low-resolution CT (Janssen et al., 2020); thus, the minor changes in tissue density associated with IB may not be detected.

The objective of this study was to determine if internal browning can be accurately detected using a single 2D CT slice at a resolution that is not high enough to detect individual cells and pores. 'Kanzi' and 'Braeburn' fruit, both IB-sensitive cultivars, were scanned with a voxel size of approximately 130 μm before and after CA storage. Fruit were visually scored on the intensity of brown tissue, and results were compared to the percentage of detectable voids in whole fruit CT slices as determined using image thresholding.

2. Materials and methods

2.1. Apple samples

In 2021, 120 'Kanzi' apple fruit were harvested at the optimal harvest date from orchards surrounding Geldermalsen, the Netherlands, and subsequently stored under CA conditions (4 °C, 1 kPa O_2, 1.5 kPa CO_2) for eight months (dataset 1). An additional 20 'Kanzi' apple fruit from the 2022 harvest year, which were stored under regular air (RA) conditions (4 °C) for approximately one month after harvest, were included as a non IB control (dataset 2). Following CA storage removal, whole fruit were scanned (Section 2.2) after one week of shelf-life at 20 °C. After CT scanning, fruit were horizontally sliced into 4 mm pieces using a meat slicer (CaterChef, EMGA, Mijdrecht, The Netherlands) equipped with a transparent acrylic sheet as the back plate. During processing, an image of each slice was captured through an acrylic sheet. The photo images were used to classify the type of browning and browning intensity for each apple. An image registration algorithm was used to align the correct CT slice with the photo image for easier comparisons (Schut et al., 2023b). CT slices and photo images of Dataset 1 can be downloaded at https://doi.org/10.5281/zenodo.8167285 (Schut et al., 2023a). Browning intensity was scored for each browning type on a subjective scale of 1 to 4, where; (1) indicates no brown tissue; (2) mild; (3) moderate and (4) severe browning intensity. Intensity scores were used to record the main type of browning for each apple. Other damage, such as cavities, decay and bruising, was also noted.

In 2022, 79 'Braeburn' apple fruit were harvested at the optimal harvest date from Randwijk experimental orchard, the Netherlands, then stored under browning-inducing CA conditions (0.5 °C, 1.5 kPa O_2, 5 kPa CO_2) for 2 and 3 months (data set 3). A subsample (32) was scanned before CA storage as a non IB control (data set 4); these fruit were stored under RA (1 °C) for two weeks after harvest before scanning. Eleven fruit were periodically removed from storage to monitor browning development. After two months, 27 fruit were removed from storage and scanned after two weeks of shelf-life. After three months, the remaining fruit were removed from CA storage, and 21 and 20 fruit were scanned after one and two weeks of shelf-life, respectively. Fruit were then sliced with a knife into approximately 10 mm slices, photographed and scored for browning intensity, as previously mentioned.

2.2. X-ray CT scanning

Whole apples were scanned using the custom FleX-ray CT-scanner (TESCAN-XRE, Gent, Belgium) (Coban et al., 2020), operated at a voxel size of approximately 130 μm. The voxel resolution was selected as a trade-off between acquisition time and image quality. CA-stored and RA-stored 'Kanzi' fruit were scanned as a voxel size of 129.3 μm and 130.6 μm, respectively. RA-stored and CA-stored 'Braeburn' fruit were scanned at a voxel size of 130.6 μm and 134.3 μm, respectively. The voxel sizes slightly differed due to a defective scanner motor, which limited the range of possible resolutions but otherwise did not affect the scans. The average time per scan was five minutes, and 1440 projection

images were captured at an exposure time of 100 ms. The tube peak voltage was 90 kV, and the current was 550 μA. Volumes were reconstructed with the FDK algorithm (Feldkamp et al., 1984). Beam hardening correction for 'Kanzi' fruit was used from the FleXbox package (Kostenko et al., 2020). Third degree polynomial beam hardening correction was used for 'Braeburn' (Herman, 1979), and the parameters were fit so that a paper cup of apple juice would not display beam hardening. The different beam hardening correction methods were used due to the replacement of the X-ray detector between the scanning of 'Kanzi' and 'Braeburn', making the parameters that were fitted on the cup of juice unusable for 'Kanzi' scans.

2.3. Image processing

Due to the voxel resolution of this study and the potential for artefacts, perfect segmentation of larger pores is limited and accurate porosity could not be calculated. However, the dark regions associated with browning in CT scans were of interest, consisting of low-density tissue containing voids or cavities and partially collapsed cells. These dark regions will be referred to as voids hereafter for simplicity.

Using every fifth CT image (~105 images per apple), the void percentage (V_p) of whole slices was calculated using the Image Batch Processor in Matlab (R2021b, The MathWorks Inc., Natick, MA). The distance between selected image slices was 0.65 mm. First, images were segmented using an adaptive threshold using Otsu's method (Otsu, 1979) (Fig. 1B). The flood fill function included the image background in the binary image with the threshold increased to remove the peel. The remaining binary image was then inverted (Fig. 1C), and the total segmented void area was calculated. The clear border and fill holes functions were applied to the binary image (Fig. 1B) to calculate the total area of the whole apple (Fig. 1D). The inverted binary image contained the seed cavity as a void area. To exclude the seed cavity region, the inverted binary image was cropped and filtered to remove small connected components that left only the seed cavity space, which was subtracted from the total void area. The centroid location of the total apple mask (Fig. 1D) was used as the centre point for cropping the seed cavity region (30 × 30 mm). Small connected components were removed using a function generated in the Image Region Analyser application. Images were filtered based on the Major Axis Length (≥ 20), Minor Axis Length (≥ 5) and Euler Number (≤ 1), and the remaining area was calculated (Fig. 1E). The following formula was used to calculate V_p;

$$V_p = \frac{C - E}{D} \quad x100$$

where C is the total void area (Fig. 1C), E is the seed cavity area after filtering (Fig. 1E), and D is the total area of the apple (Fig. 1D). 3D images were created using Volume Viewer in Matlab.

2.4. Density measurements

Fruit density was measured to confirm that V_p was related to air-filled voids. Density measurements were performed on 'Braeburn' fruit stored for three months, one day after CT scanning. A large container with room temperature water was placed on a scale with a cage suspended from a retort stand and submerged in the water. Fruit were weighed (W_0) in air and then placed inside the submerged cage, and the weight of the displaced water (W_1) was recorded. Fruit density was calculated as W_0/W_1 in kg m^{-3}.

2.5. Statistical analysis

All data were subjected to analysis of variance (ANOVA), and the means of the browning intensity scores and cultivar were compared by Tukey's HSD test ($p < 0.05$). A two-tailed Person's correlation ($p < 0.05$) was performed for correlation analysis. The V_p values calculated from CT images at 5 mm intervals, ranging from 5 and 50 mm from the stem end, were used for classification analysis to determine the optimum CT slice for IB detection. A 5-fold cross-validation approach was used to assess the performance of the logistic regression models for each slice distance. The dataset, containing both cultivars and datasets (CA-stored and RA-stored), was divided into five subsets using the 'createFolds' function. For each fold, a binomial logistic regression model was trained using the 'glm' function. The affected/healthy status served as the dependent variable and the V_p at a specific distance as the independent variable. Predictions were generated for one fold (testing set) using the logistic regression model trained on the remaining four folds (training set). Class labels (0 or 1) were assigned based on a threshold of 0.5 applied to the predicted probabilities. True positives (TP) represent correctly classified affected fruit; true negatives (TN) represent correctly classified healthy fruit; false positives (FP) represent healthy fruit incorrectly classified as brown; and false negatives represent affected fruit incorrectly classified as healthy. The evaluation metrics, sensitivity [TP / (TP + FN)], specificity [TN / (TN + FP)], misclassification rate [(FP + FN) / (TP + TN + FP + FN)] and area under the receiver operating characteristic curve (AUC) were calculated for each fold to assess the performance of the models. Sensitivity (or true positive rate) measures the model's ability to identify affected fruit correctly with a value closer to 1 indicating accurate classification. Specificity (or true negative rate) measures the model's ability to correctly identify healthy fruit with a value closer to 1 indicating a low false positive rate. The misclassification rate (or error rate) quantifies the proportion of incorrectly classified instances; a lower misclassification rate indicates a better overall model performance. An AUC value close to 1 indicates the model has a good ability to distinguish between affected and healthy fruit. All analyses were performed using the statistical software R version 4.0.2 (R Core Team, 2023).

3. Results

3.1. Browning

All 20 RA-stored 'Kanzi' fruit (dataset 2) were free from disease and disorders. Of the 120 CA-stored samples (dataset 1), 36% of fruit were

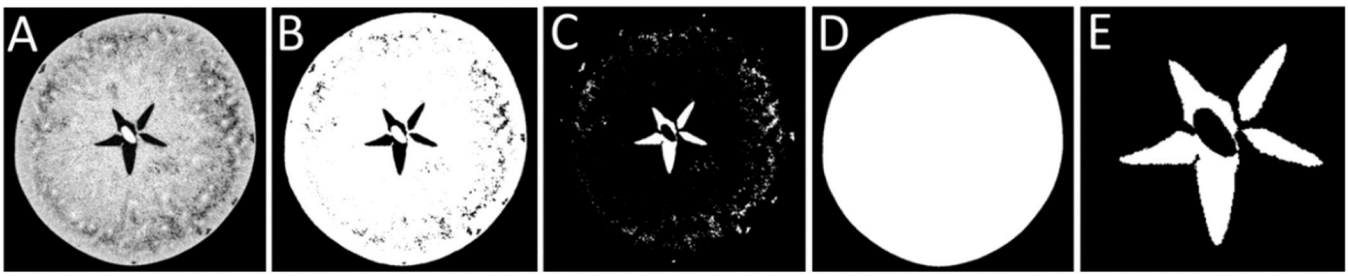

Fig. 1. Performance illustration of thresholding method: (A) original image; (B) binary image obtained using an adaptive threshold (Otsu's method); (C) inverted binary image; (D) binary image of total apple size; (E) inverted binary image of cropped seed cavity after filtering.

healthy, 63% contained brown tissue, and 2% were completely rotten and excluded from the analysis. The percentage of fruit in each browning intensity class was (1) 14 (RA-stored) and 31 (CA-stored fruit); (2) 16; (3) 11; (4) 26. The predominant type of browning was 'both' (radial and core; 46%), followed by senescent breakdown (7%), core browning (4%), radial browning (3%) and diffuse flesh browning (3%). An example of each browning type is presented in Fig. 2, and the 3D visualisation is in Fig. 3. The main damage, other than browning, was bruising (33%), followed by small cavities (27%) and decay (8%).

The percentage of 'Braeburn' fruit with core browning after two months of storage was 44%. After three months of storage, the percentage of affected fruit was 71% and 85% after one and two weeks of shelf-life, respectively. The percentage of the 68 CA-stored fruit in each browning intensity class was (1) 35; (2) 21; (3) 22; (4) 22. Radial browning was observed in 33% and 53% of fruit with an intensity score of 3 and 4, respectively. The main damage other than browning was decay (13%), followed by bitter pit (10%), bruising (7%) and cavities (4%). For some healthy 'Braeburn' fruit, dark regions surrounding the core that developed during CA storage were visible in CT scans; however, no brown tissue was detected during slicing (Fig. 4B & C). A similar trend occurred in some affected 'Braeburn' fruit, where dark regions in CT scans did not always correspond to brown tissue (Fig. 4E & H).

3.2. Image analysis

The V_p was calculated using Otsu's method for thresholding for every fifth CT image per fruit from the stem end to the calyx. The average V_p for each intensity class at each distance is presented in Fig. 5 and excludes fruit with other damage unrelated to internal browning (decay and bruising). After exclusions, the number of 'Kanzi' fruit in each browning intensity class in Fig. 5A was (1) 20 RA-stored and 23 CA-stored fruit; (2) 12; (3) 11; (4) 30. The number of 'Braeburn' fruit in each browning intensity class in Fig. 5B was (1) 30 RA-stored and 15 CA-stored fruit; (2) 10; (3) 10; (4) 10. The greatest variation in V_p among browning intensity classes was within the first 20 mm of 'Kanzi' fruit stem end (Fig. 5A). For affected 'Kanzi' fruit, the highest V_p for each browning score was about 10 mm from the stem end, with V_p decreasing towards the calyx thereafter. The largest variation in V_p among browning intensity classes was between 30 and 40 mm of 'Braeburn' fruit stem end (Fig. 5B). Fruit with severe browning intensity (4) had a higher V_p in the tissue preceding the core (10 and 25 mm of the stem-end) than fruit with less intense browning (2 and 3) and healthy fruit. For both cultivars, CA-stored healthy fruit had a higher V_p than RA-stored healthy fruit ($p < 0.05$) (Fig. 5).

A classification of fruit health status (healthy or brown) after storage was made by performing a 5-fold cross-validation using V_p at a specific distance from the stem as the independent variable (Table 1). The model using the V_p of CT slices 35 mm from the fruit's stem end had the best ability to distinguish between affected and healthy fruit, as indicated by having the highest AUC value. The V_p at 35 mm also showed the highest sensitivity rate and the lowest misclassification rate than the models at other distances (Table 1). The models using V_p of CT slices 30 and 35 mm from the fruit's stem end showed better predictive performance than the model using the average V_p of the whole apple (Table 1).

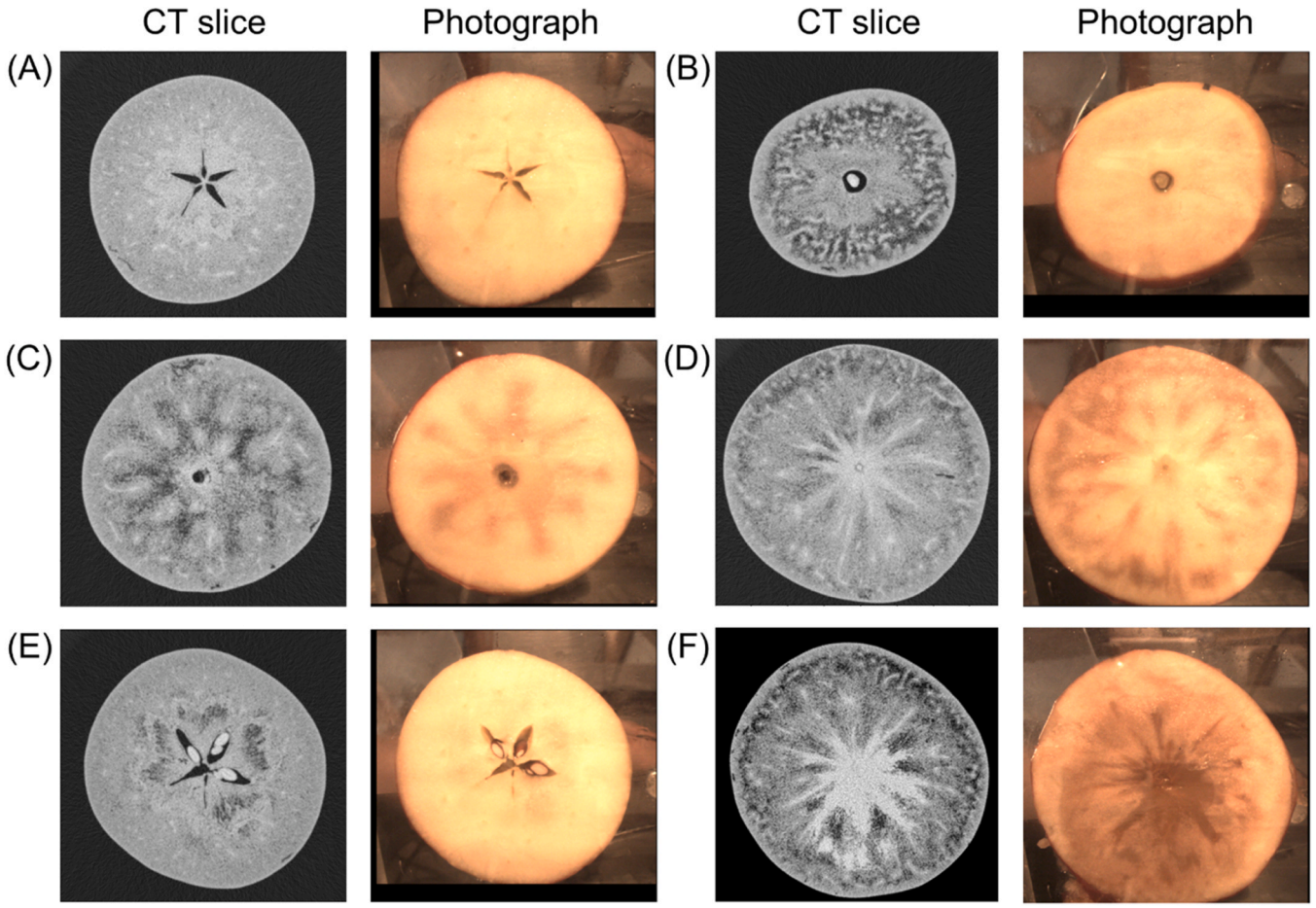

Fig. 2. CT slice images (left) of a healthy (A) 'Kanzi' apple and fruit with different types of flesh browning and the corresponding photograph (right). The types of browning identified were (B) senescent breakdown, (C) radial browning, (D) diffuse flesh browning, (E) core browning and (F) browning due to decay. 3D visualisation of apples A-E are presented in Fig. 3.
(A) adapted from Schut et al. (2023b).

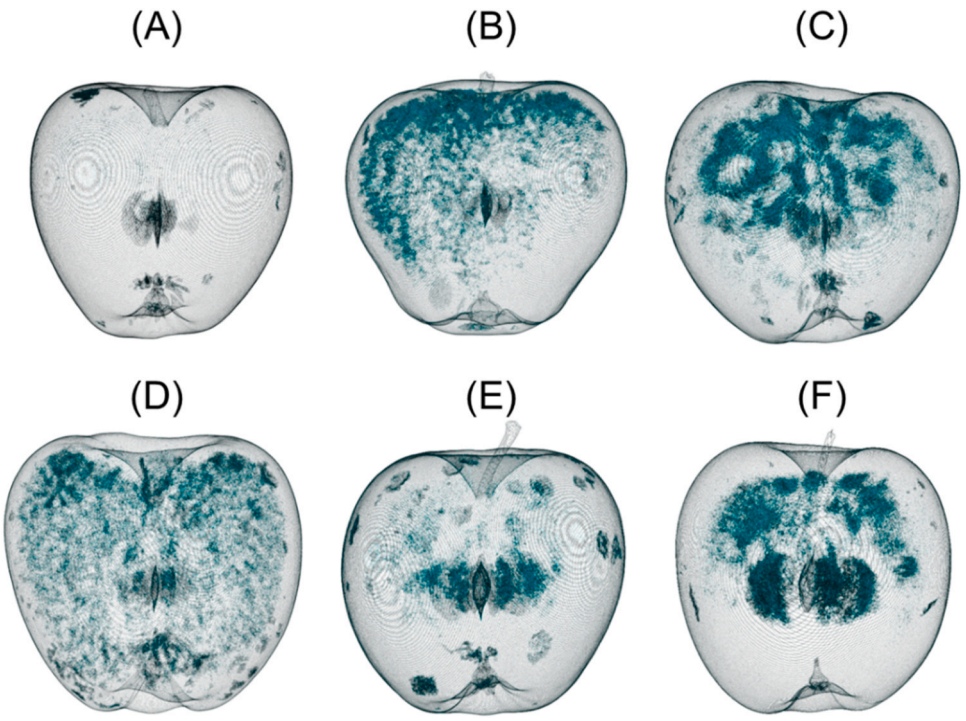

Fig. 3. 3D visualisation of a healthy 'Kanzi' apple (A) and 'Kanzi' fruit with different types of browning (B-E) that are shown in 2D in Fig. 2. The affected tissue is displayed in blue. The types of browning were (B) senescent breakdown, (C) radial browning, (D) diffuse flesh browning, (E) core browning and (F) 'Braeburn' apple with core and radial browning.

The average V_p increased as browning intensity increased in 'Kanzi' and 'Braeburn' fruit (Fig. 6). In each browning class, 71% of the outliers for 'Kanzi' and 88% for 'Braeburn' fruit also contained other damage (Fig. 6). The presence of cavities and decay caused the largest increase in V_p from the mean for the 'Kanzi' data set. For 'Braeburn', decay and bruising caused the largest increase in V_p from the mean. Healthy 'Kanzi' fruit had a lower average V_p than 'Kanzi' fruit with brown tissue (Fig. 6A). For 'Braeburn', the V_p of fruit with mild browning intensity (2) did not differ from healthy fruit (Fig. 6B). When the average V_p from only the core region was analysed (grey region in Fig. 5), healthy 'Braeburn' fruit differed from fruit with mild browning intensity (data not shown). For CA-stored fruit, the average V_p showed a weak positive relationship with apple width (total mask area; Fig. 1D) (Kanzi, $r = 0.39$, $p < 0.001$; Braeburn, $r = 0.24$, $p = 0.05$). 'Kanzi' fruit with an intensity score of 4 (severe) were 7% and 8% larger (sum of total mask area) than fruit with a browning intensity of 1 and 2, respectively (data not shown). For 'Braeburn', fruit size did not differ among intensity scores (data not shown). There was no difference in the V_p of RA-stored fruit (data sets 2 & 4) between cultivars ($p > 0.05$). For CA-stored fruit (data sets 1 & 3), 'Kanzi' had a higher average V_p than 'Braeburn' ($p < 0.05$).

3.3. Density measurements

The density (kg m^{-3}) of 'Braeburn' fruit stored for three months had a negative relationship with the average V_p ($R = -0.50$, $p < 0.001$), which was stronger when fruit with other damage were removed from the analysis ($R = -0.65$, $p < 0.01$). Density decreased as browning intensity increased (Fig. 7).

4. Discussion

4.1. Browning detection

Internal browning (IB) intensity in CA-stored 'Kanzi' and 'Braeburn' fruit was related to the percentage of segmented voids in CT slices with a voxel size of approximately 130 μm, as determined via image thresholding. As the intensity of brown tissue in an apple increased, the average void percentage (V_p) increased. For both cultivars, ≥ 71% of the outliers with a higher V_p than the average for each browning intensity score also contained other damage. The presence of decay and cavities caused the greatest increase in V_p from the browning intensity score mean for 'Kanzi' fruit, whereas decay and bruising caused the greatest increase for 'Braeburn' fruit. These results indicate that V_p detects damaged tissue rather than only enzymatic browning. Indeed, Diels et al. (2017) used a similar thresholding method to detect and quantify bruised tissue in multiple apple cultivars using CT with a voxel size of 211 μm. They segmented the bruised tissue in CT images using the multi-level Otsu's threshold method; however, the bruises were highly irregular in shape and bruise volume estimations based on simple geometric assumptions could not deliver accurate results (Diels et al., 2017). Our method does not rely on the shape of the affected tissue to quantify damage, likely contributing to the high accuracy of our results.

For 'Kanzi' fruit, the greatest variation in V_p among browning classes was within the first 20 mm from the fruit stem end. These results were due to the high incidence of radial flesh browning (RFB) within samples, where affected tissue is highest at the stem end of fruit and decreases towards the core and calyx (James and Jobling, 2009). Furthermore, 73% of affected fruit contained RFB and core browning with equal intensity. RFB was also observed in 'Braeburn' fruit with severe browning. Generally, apples are cut transversally through the equatorial region during disorder inspection (Kittemann et al., 2015; Weber et al., 2019; Wood et al., 2022); thus, incidences of RFB would be missed as affected tissue is highest at the stem end. Our results indicate that RFB and core browning likely co-occur in 'Kanzi' fruit and with severe core browning in 'Braeburn' fruit grown in the Netherlands. RFB was not previously reported to occur in both 'Kanzi' and 'Braeburn' fruit. Further research should determine if RFB occurs with CB in 'Kanzi' and 'Braeburn' fruit produced in other apple growing regions.

The greatest variation in V_p among browning classes for 'Braeburn'

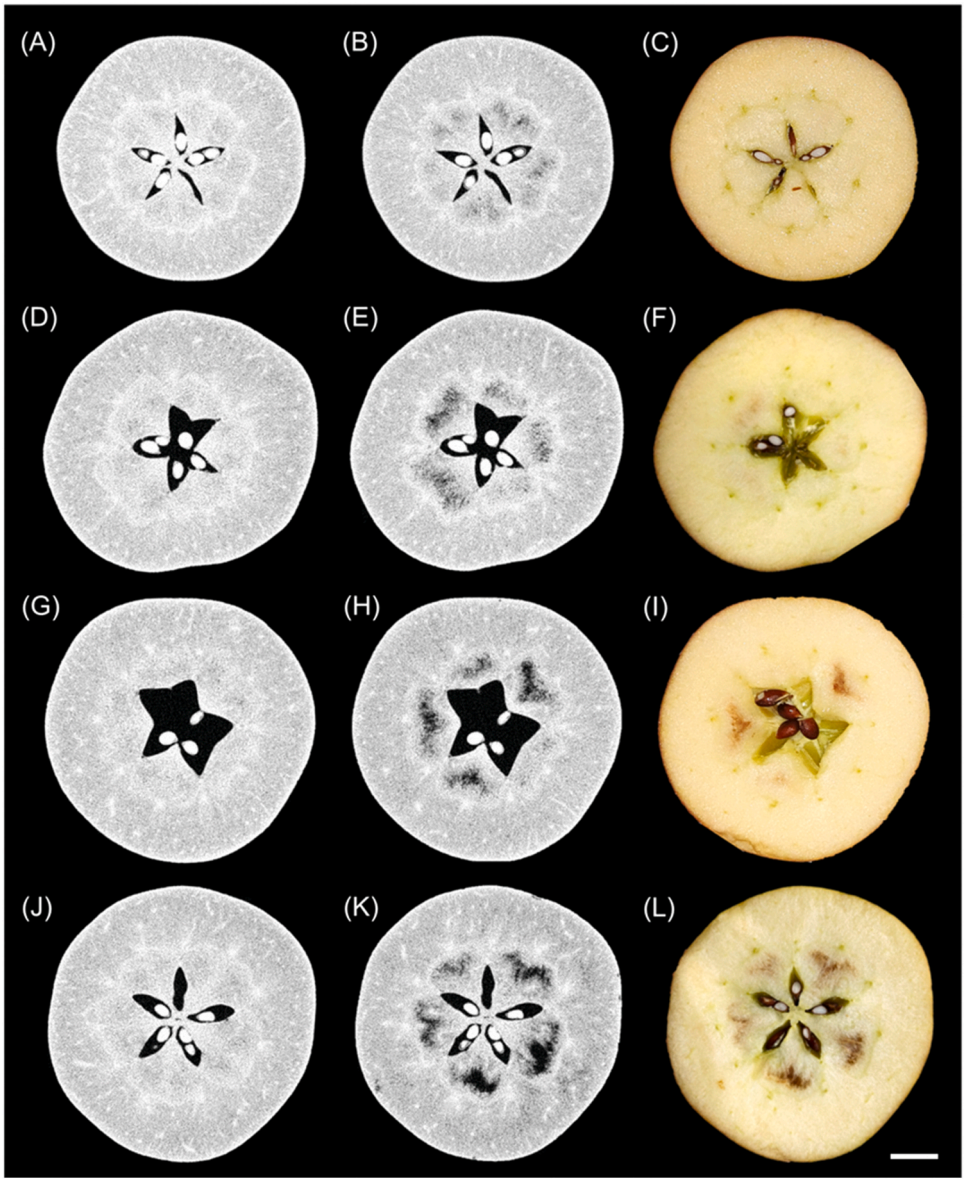

Fig. 4. CT scans of 'Braeburn' fruit before (left) and after (middle) CA storage and the corresponding photo image after storage (right). The browning intensity scores of each apple (based on the whole fruit) after storage were B/C = 1, E/F = 2, H/I = 3, K/L = 4. Scale bar measures 1 cm.

fruit occurred within the core region (between 30 and 40 mm from the stem end). Accordingly, the models with the best predictive performance for classifying affected fruit (both cultivars) were at 30 and 35 mm from the stem end of fruit (Table 1). Furthermore, the accuracy of the models using V_p of CT slices at 30 and 35 mm was higher than the model using the average V_p of the whole fruit (Table 1). These results indicate that the whole apple does not need to be analysed for browning classification, which would greatly reduce image processing time. Using one X-ray image at a predetermined location has a greater potential for practical applications (Kotwaliwale et al., 2014), and for our data set, the optimal location for IB classification using one 2D CT scan was 35 mm from the fruit stem end. The scanning time of this study was five minutes, which is substantially lower than previous studies investigating internal browning in apples; however, the scanning time is very dependent on the scanner used. This study was conducted on a laboratory scanner, but in practice, multiple X-ray sources or a higher-powered X-ray source would be needed to increase the acquisition speed. Therefore, before in-line sorting can occur, a CT scanning setup should be designed that satisfies the requirements for cost, scanning time, and image quality. Scanning one CT slice may reduce the cost compared to 3D scanning by using a smaller X-ray detector.

For 'Braeburn', CB incidence increased with the storage duration, further exacerbated by the shelf life duration, consistent with the literature on other browning disorders (Meheriuk et al., 1994; Sidhu et al., 2023). Despite the high CO_2 partial pressure during storage, only CB was detected in 'Braeburn' fruit, excluding RFB. Elgar et al. (1998) also stored 'Braeburn' fruit at 5 kPa CO_2 and observed incidences of CB and Braeburn Browning Disorder (BBD), a disorder that affects the outer flesh between the skin and the core region. However, they reported a significant reduction in BBD when the establishment of CA storage had a two-week delay. In this study, fruit did not show BBD symptoms, likely due to the two-week delay in CA establishment. As it is standard practice to delay CA establishment for the long-term storage of 'Braeburn' apple, the flesh browning observed in this study is similar to that observed in industry.

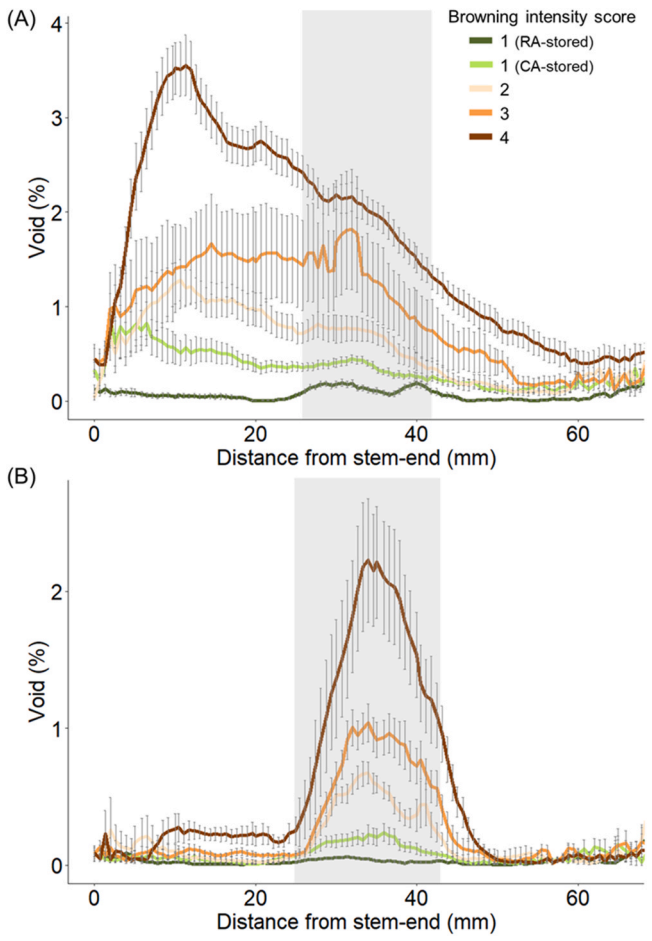

Fig. 5. The void percentage (V_p) of CT slices of healthy (A) 'Kanzi' and (B) 'Braeburn' fruit and fruit with internal browning. An intensity score of (1) indicates no brown tissue (CA-stored and RA-stored); (2) mild; (3) moderate; and (4) severe browning. Data is of every fifth CT slice, and fruit with bruising and decay were removed. The grey shaded box indicates the average core area. The standard error of the mean is denoted by capped bars.

4.2. Browning is positively linked to porosity

Although the voxel size in this study was more than double that of previous IB reports in apples (~130 μm vs. ~60 μm) (Chigwaya et al., 2021b; Herremans et al., 2013), the dark regions associated with IB were still visible in CT scans. CT with a voxel resolution of 45 μm cannot detect smaller pores (Janssen et al., 2020); however, Janssen et al. (2020) reported that porosity does not differ between images captured using low- and high-resolution CT when using image thresholding. Furthermore, only about 5% and 10% of pores are less than 125 μm in 'Braeburn' and 'Kanzi' fruit, respectively (Herremans et al., 2015). Therefore, the V_p calculated in this study is likely positively associated with porosity; thus, IB intensity increases with increasing porosity. Indeed, the density of 'Braeburn' fruit, which is inversely related to porosity (Herremans et al., 2015; Janssen et al., 2020), was negatively correlated with the average V_p, and density decreased as browning intensity increased. These results are consistent with Nugraha et al. (2022) study on pears, which reported that porosity was higher for affected fruit than healthy fruit after eight months of CA storage. However, Chigwaya et al. (2021b) noted that the porosity of 'Fuji' apples stored under browning-inducing conditions was lower in brown tissue than in healthy tissue. Although, fruit in Chigwaya et al. (2021b) study were only exposed to unfavourable conditions for three days. Herremans et al. (2013) demonstrated that pores are flooded during the early stages of browning before water moves away from affected areas and cells begin to collapse. In this study, fruit were scanned after several months of CA storage; thus, affected fruit would be in the late stages of browning when cells have collapsed, and water has moved away from affected tissue, increasing porosity and V_p.

For both cultivars, healthy CA-stored fruit had a higher V_p than healthy RA-stored fruit, indicating that fruit tissue structure changes during CA storage, as shown in Fig. 4A-B. Similar results were reported by Herremans et al. (2013), who noted considerably larger pores in 'Braeburn' apples stored longer than 100 days than fruit before CA storage; however, the overall porosity was not greatly affected. They suggested that larger pores are formed by connecting previously present pores, possibly due to a loss of cell-to-cell adhesion. A loss of cell-to-cell adhesion occurs during the ageing process and is accompanied by moisture loss, reduced crunchiness and an increased sensation of mealiness (Herremans et al., 2013). As smaller pores are not detected with low-resolution CT as previously discussed, the increase in V_p during CA storage in healthy fruit likely occurred due to the connection of small pores ($\leq$ 130 μm) rather than tissue breakdown, which were then detectable at our selected resolution. Indeed, a greater percentage of small pores occur closer to the ovary than the outer tissue (Janssen et al., 2020), and it was at this location that dark regions formed in healthy 'Braeburn' fruit during CA storage.

For affected 'Braeburn' fruit, dark regions within the inner cortex visible in CT scans did not always correspond to brown tissue. However, affected fruit had a lower density and higher V_p than healthy fruit. Mealiness is reported as the last stage of texture degradation before internal breakdown and browning (Barreiro et al., 1999). Harker and Hallett (1992) suggested that high levels of intercellular air-filled spaces are likely a symptom of mealiness. Indeed, researchers have reported that the proportion of large pores measured using micro-CT (voxel size $\leq$ 10 μm) increased with the degree of mealiness in apples (Iida et al., 2023) and pears (Muziri et al., 2016). Therefore, perhaps the regions of flesh that were dark in CT scans but not brown were mealy. These results suggest that the early stages of internal browning when water moves away from affected regions before cell breakdown and the formation of larger voids may be visible in CT scans. The early detection of browning would be extremely valuable for shelf-life quality predictions as browning can progressively worsen at room temperature after removal from CA storage (Meheriuk et al., 1994). Accordingly, fruit with dark regions in the CT scans but without browning may have been mealy and developed enzymatic browning over a longer shelf-life. However, further studies are needed to monitor the development of core browning

Table 1
Average classification results for logistic regression models using V_p at each distance from the stem-end for classifying affected fruit in 5-fold cross validation*.

Evaluation metric	Distance from the stem end (mm)										Whole fruit average
	5	10	15	20	25	30	35	40	45	50	
Sensitivity	0.46	0.60	0.59	0.61	0.63	0.80	0.84	0.75	0.54	0.47	0.72
Specificity	0.83	0.89	0.87	0.89	0.87	0.84	0.86	0.82	0.85	0.88	0.85
Misclassification rate	0.36	0.25	0.27	0.25	0.25	0.18	0.15	0.22	0.30	0.33	0.22
AUC	0.72	0.81	0.84	0.85	0.84	0.91	0.94	0.89	0.80	0.75	0.89

* Sensitivity: values closer to 1 indicate accurate classification. Specificity: values closer to 1 indicate a low false positive rate. Misclassification rate: lower values indicate a better overall model performance. AUC: values close to 1 indicate the model can distinguish between affected and healthy fruit effectivity.

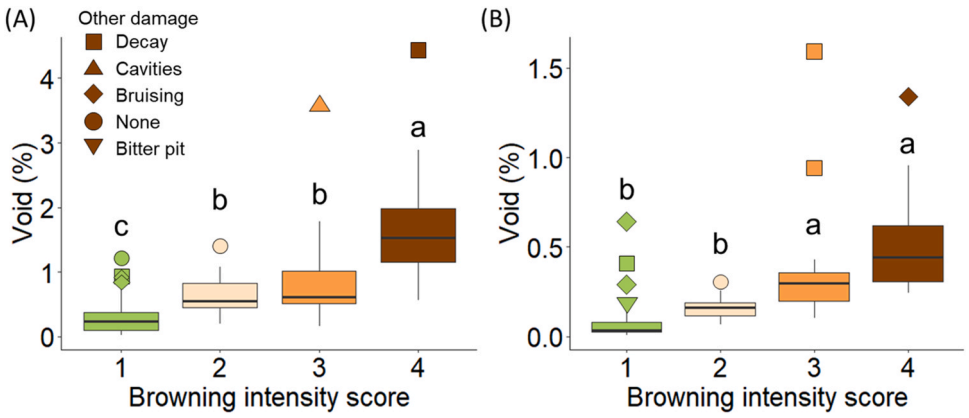

Fig. 6. Box plot of the average void percentage (V_p) calculated from CT scans of (A) 'Kanzi' and (B) 'Braeburn' fruit with different browning intensity scores. Data are pooled for CA-stored and RA-stored healthy fruit. Bars with different letters are significantly different ($p < 0.05$). The centre line in each box represents the median value, the top and bottom of the box correspond to the 25th and 75th percentiles, and the whiskers represent the 10th and 90th percentiles. Outliers beyond the whiskers are shown as individual points, and their shape indicates if fruit contained damage other than browning.

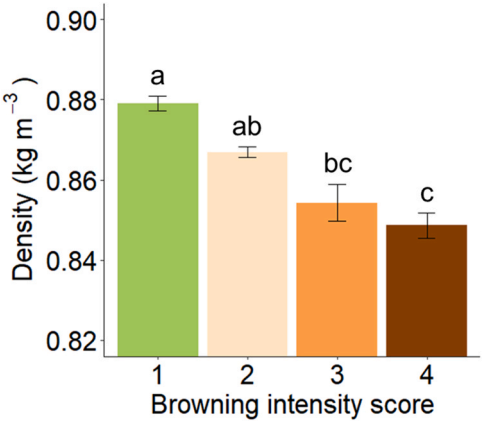

Fig. 7. The density of 'Braeburn' fruit with different browning intensity scores after three months of CA storage. Bars with different letters are significantly different ($p < 0.05$). The standard error of the mean is denoted by a capped bar at the top of each column.

in whole fruit to confirm this notion.

5. Conclusion

This study showed that CT with a voxel size of approximately 130 μm could accurately detect internal browning in 'Kanzi' and 'Braeburn' fruit using a single 2D slice (AUC of 0.94 at 35 mm from the stem). The percentage of segmented voids calculated from binary images increased as the intensity of brown tissue increased. Radial flesh and core browning occurred concurrently in CA-stored 'Kanzi' fruit and in 'Braeburn' fruit with severe core browning. Linear regression models using the void percentage of CT slices at 30 and 35 mm of the fruit stem end had a better predictive performance for classifying affected fruit than models using the whole fruit average. These results demonstrate that the entire fruit does not need to be analysed for accurate classification. Using only a few CT slices per fruit would greatly reduce image analysis time, which is imperative for realising in-line non-destructive quality analysis using CT. Our results indicated that void percentage could also be used to identify other damaged tissue such as decay, bruising and cavities. Deriving additional features from the CT image may enhance the model's predictive performance. Nevertheless, the results of this study provide a foundation for future research and demonstrate the feasibility of using void percentage calculated from low-resolution CT scans to detect internal browning in 'Kanzi' and 'Braeburn' apples. However, further research is needed to determine the differences in void percentage between fruit undergoing natural senescence and fruit with internal browning.

Funding

This publication is part of the project Utopia (ENWSS.2018.003) of the research programme Smart Solutions for horti- and agriculture, which is partly financed by the Dutch Research Council (NWO).

CRediT authorship contribution statement

Rachael M. Wood: Writing – review & editing, Writing – original draft, Visualization, Software, Methodology, Investigation, Formal analysis, Data curation, Conceptualization. **Dirk Schut:** Writing – review & editing, Writing – original draft, Software, Methodology, Investigation, Conceptualization. **Anna Trull:** Writing – review & editing, Resources, Methodology, Investigation, Conceptualization. **Leo Marcelis:** Writing – review & editing, Supervision, Funding acquisition. **Rob Schouten:** Writing – review & editing, Writing – original draft, Supervision, Funding acquisition, Conceptualization.

Declaration of Generative AI and AI-assisted technologies in the writing process

During the preparation of this work the authors used ChatGPT in order to improve the manuscripts readability. After using this tool/service, the authors reviewed and edited the content as needed and takes full responsibility for the content of the publication.

Declaration of Competing Interest

The authors declare that they have no known competing financial interests or personal relationships that could have appeared to influence the work reported in this paper.

Data Availability

Data will be made available on request.

Acknowledgements

The authors would like to acknowledge Michiel Couvée for technical assistance with 'Kanzi' fruit slicing. Authors would also like to thank FruitMasters™, and Peter Balk and Alma van der Heiden from

Wageningen Plant Research in Randwijk for providing fruit samples.

References

Barreiro, P., Ruiz–Cabello, J., Fernández–Valle, M.E., Ortiz, C., Ruiz–Altisent, M., 1999. Mealiness assessment in apples using MRI techniques. Magn. Reson Imaging 17, 275–281. https://doi.org/10.1016/s0730-725x(98)00160-x.

Buzug, T., 2008. Computed Tomography: From Photon Statistics to Modern Cone-Beam CT. Springer, Berlin, Heidelberg. https://doi.org/10.1007/978-3-540-39408-2.

Chigwaya, K., Karuppanapandian, T., Schoeman, L., Viljoen, D.W., Crouch, I.J., Nugraha, B., Verboven, P., Nicolaï, B.M., Crouch, E.M., 2021a. X-ray CT and porosity mapping to determine the effect of 'Fuji' apple morphological and microstructural properties on the incidence of CO_2 induced internal browning. Postharvest Biol. Technol. 174, 111464 https://doi.org/10.1016/j.postharvbio.2021.111464.

Chigwaya, K., Plessis, A. du, Viljoen, D.W., Crouch, I.J., Crouch, E.M., 2021b. Use of X-ray computed tomography and 3D image analysis to characterize internal browning in 'Fuji' apples after exposure to CO_2 stress. Sci. Hortic. 277, 109840 https://doi.org/10.1016/j.scienta.2020.109840.

Clark, C.J., McGlone, V.A., Jordan, R.B., 2003. Detection of Brownheart in 'Braeburn' apple by transmission NIR spectroscopy. Postharvest Biol. Technol. 28, 87–96. https://doi.org/10.1016/S0925-5214(02)00122-9.

Coban, S.B., Lucka, F., Palenstijn, W.J., Van Loo, D., Batenburg, K.J., 2020. Explorative Imaging and Its Implementation at the FleX-ray Laboratory. J. Imaging 6, 18. https://doi.org/10.3390/jimaging6040018.

Crowther, R.A., DeRosier, D.J., Klug, A., 1970. The reconstruction of a three-dimensional structure from projections and its application to electron microscopy. Proc. R. Soc. Lond. A. Math. Phys. Sci. 317, 319–340. https://doi.org/10.1098/rspa.1970.0119.

Diels, E., van Dael, M., Keresztes, J., Vanmaercke, S., Verboven, P., Nicolai, B., Saeys, W., Ramon, H., Smeets, B., 2017. Assessment of bruise volumes in apples using X-ray computed tomography. Postharvest Biol. Technol. 128, 24–32. https://doi.org/10.1016/j.postharvbio.2017.01.013.

Elgar, H.J., Burmeister, D.M., Watkins, C.B., 1998. Storage and handling effects on a CO_2-related internal browning disorder of "braeburn" apples. HortScience 33, 719–722. https://doi.org/10.21273/hortsci.33.4.719.

Feldkamp, L.A., Davis, L.C., Kress, J.W., 1984. Practical cone-beam algorithm. J. Opt. Soc. Am. A 1, 612. https://doi.org/10.1364/JOSAA.1.000612.

Han, D., Tu, R., Lu, C., Liu, X., Wen, Z., 2006. Nondestructive detection of brown core in the Chinese pear 'Yali' by transmission visible–NIR spectroscopy. Food Control 17, 604–608. https://doi.org/10.1016/j.foodcont.2005.03.006.

Harker, F.R., Hallett, I.C., 1992. Physiological changes associated with development of mealiness of apple fruit during cool storage. HortScience 27, 1291–1294. https://doi.org/10.21273/hortsci.27.12.1291.

Hatoum, D., Buts, K., Hertog, M., Geeraerd, A.H., Schenk, A., Vercammen, J., Nicolai, B. M., 2014. Effects of pre- and postharvest factors on browning in Braeburn. Hortic. Sci. 41, 19–26. https://doi.org/10.17221/180/2013-HORTSCI.

Herman, G.T., 1979. Correction for beam hardening in computed tomography. Phys. Med. Biol. 24, 008. https://doi.org/10.1088/0031-9155/24/1/008.

Herremans, E., Verboven, P., Bongaers, E., Estrade, P., Verlinden, B.E., Wevers, M., Hertog, M., Nicolai, B.M., 2013. Characterisation of 'Braeburn' browning disorder by means of X-ray micro-CT. Postharvest Biol. Technol. 75, 114–124. https://doi.org/10.1016/j.postharvbio.2012.08.008.

Herremans, E., Verboven, P., Verlinden, B.E., Cantre, D., Abera, M., Wevers, M., Nicolaï, B.M., 2015. Automatic analysis of the 3-D microstructure of fruit parenchyma tissue using X-ray micro-CT explains differences in aeration. BMC Plant Biol. 15, 264 https://doi.org/10.1186/s12870-015-0650-y.

Huang, Y., Lu, R., Chen, K., 2020. Detection of internal defect of apples by a multichannel Vis/NIR spectroscopic system. Postharvest Biol. Technol. 161, 111065 https://doi.org/10.1016/j.postharvbio.2019.111065.

Iida, D., Kokawa, M., Kitamura, Y., 2023. Estimation of apple mealiness by means of laser scattering measurement. Food Bioproc. Tech. https://doi.org/10.1007/s11947-023-03068-3.

James, H.J., Jobling, J.J., 2009. Contrasting the structure and morphology of the radial and diffuse flesh browning disorders and CO_2 injury of 'Cripps Pink' apples. Postharvest Biol. Technol. 53, 36–42. https://doi.org/10.1016/j.postharvbio.2009.02.001.

Janssen, S., Verboven, P., Nugraha, B., Wang, Z., Boone, M., Josipovic, I., Nicolaï, B.M., 2020. 3D pore structure analysis of intact 'Braeburn' apples using X-ray micro-CT. Postharvest Biol. Technol. 159, 111014 https://doi.org/10.1016/j.postharvbio.2019.111014.

Khatiwada, B.P., Subedi, P.P., Hayes, C., Carlos, L.C.C., Walsh, K.B., 2016. Assessment of internal flesh browning in intact apple using visible-short wave near infrared spectroscopy. Postharvest Biol. Technol. 120, 103–111. https://doi.org/10.1016/j.postharvbio.2016.06.001.

Kittemann, D., Neuwald, D.A., Streif, J., 2015. Internal browning in "Kanzi®" apples - reasons and possibilities to reduce the disorder. Acta Hortic. 1079, 409–414. https://doi.org/10.17660/ActaHortic.2015.1079.52.

Kostenko, A., Palenstijn, W.J., Coban, S.B., Hendriksen, A.A., van Liere, R., Batenburg, K. J., 2020. Prototyping X-ray tomographic reconstruction pipelines with FleXbox. SoftwareX 11, 100364. https://doi.org/10.1016/j.softx.2019.100364.

Kotwaliwale, N., Singh, K., Kalne, A., Jha, S.N., Seth, N., Kar, A., 2014. X-ray imaging methods for internal quality evaluation of agricultural produce. J. Food Sci. Technol. 51, 1–15. https://doi.org/10.1007/s13197-011-0485-y.

Lammertyn, J., Dresselaers, T., van Hecke, P., Jancsók, P., Wevers, M., Nicolaï, B.M., 2003. Analysis of the time course of core breakdown in 'Conference' pears by means of MRI and X-ray CT. Postharvest Biol. Technol. 29, 19–28. https://doi.org/10.1016/S0925-5214(02)00212-0.

Lee, J., Mattheis, J.P., Rudell, D.R., 2013. Fruit size affects physiological attributes and storage disorders in cold-stored 'royal gala' apples. HortScience 48, 1518–1524. https://doi.org/10.21273/HORTSCI.48.12.1518.

Meheriuk, M., Prange, R.K., Lidster, P.D., Porritt, S.W., 1994. Postharvest Disorders of Apples and Pears. Agriculture and Agri-Food Canada, Ottawa. https://doi.org/10.5962/bhl.title.59498.

Muziri, T., Theron, K.I., Cantre, D., Wang, Z., Verboven, P., Nicolai, B.M., Crouch, E.M., 2016. Microstructure analysis and detection of mealiness in 'Forelle' pear (Pyrus communis L.) by means of X-ray computed tomography. Postharvest Biol. Technol. 120, 145–156. https://doi.org/10.1016/j.postharvbio.2016.06.006.

Nicolaï, B.M., Defraeye, T., de Ketelaere, B., Herremans, E., Hertog, M., Saeys, W., Torricelli, A., Vandendriessche, T., Verboven, P., 2014. Nondestructive measurement of fruit and vegetable quality. Annu Rev. Food Sci. Technol. 5, 285–312. https://doi.org/10.1146/annurev-food-030713-092410.

Nicolas, J.J., Richard-Forget, F.C., Goupy, P.M., Amiot, M., Aubert, S.Y., 1994. Enzymatic browning reactions in apple and apple products. Crit. Rev. Food Sci. Nutr. 34, 109–157. https://doi.org/10.1080/10408399409527653.

Nugraha, B., Verboven, P., Janssen, S., Wang, Z., Nicolaï, B.M., 2019. Non-destructive porosity mapping of fruit and vegetables using X-ray CT. Postharvest Biol. Technol. 150, 80–88. https://doi.org/10.1016/j.postharvbio.2018.12.016.

Nugraha, B., Verboven, P., Verlinden, B.E., Verreydt, C., Boone, M., Josipovic, I., Nicolaï, B.M., 2022. Gas exchange model using heterogeneous diffusivity to study internal browning in 'conference' pear. Postharvest Biol. Technol. 191, 111985 https://doi.org/10.1016/j.postharvbio.2022.111985.

Otsu, N., 1979. A threshold selection method from gray-level histograms. IEEE Trans. Syst. Man Cyber 9, 62–66. https://doi.org/10.1109/TSMC.1979.4310076.

Peirs, A., Scheerlinck, N., Touchant, K., Nicolaï, B.M., 2002. PH-postharvest technology. Biosyst. Eng. 81, 305–311. https://doi.org/10.1006/bioe.2001.0040.

R. Core Team, 2023. R: A language and environment for statistical computing. R Foundation for Statistical Computing.

Schut, D.E., Batenburg, K.J., van Liere, R., van Leeuwen, T., 2022. TOP-CT: trajectory with overlapping projections X-ray computed tomography. IEEE Trans. Comput. Imaging 8, 598–608. https://doi.org/10.1109/TCI.2022.3192125.

Schut, D.E., Trull, A.K., Couvée, M., 2023a. Dataset of CT scans, slice photographs, and visual browning scores of 120 "Kanzi" apples. https://doi.org/10.5281/zenodo.8167285.

Schut, D.E., Wood, R.M., Trull, A.K., Schouten, R., van Liere, R., van Leeuwen, T., Batenburg, K.J., 2023b. Joint 2D to 3D image registration workflow for comparing multiple slice photographs and CT scans of apple fruit with internal disorders. arXiv preprint arXiv:2310.01987.

Sidhu, R.S., Bound, S.A., Swarts, N.D., 2023. Internal flesh browning in apple and its predisposing factors—a review. Physiologia 3, 145–172. https://doi.org/10.3390/physiologia3020012.

van Dael, M., Verboven, P., Zanella, A., Sijbers, J., Nicolai, B., 2019. Combination of shape and X-ray inspection for apple internal quality control: in silico analysis of the methodology based on X-ray computed tomography. Postharvest Biol. Technol. 148, 218–227. https://doi.org/10.1016/j.postharvbio.2018.05.020.

Van De Looverbosch, T., He, J., Tempelaere, A., Kelchtermans, K., Verboven, P., Tuytelaars, T., Sijbers, J., Nicolai, B., 2022. Inline nondestructive internal disorder detection in pear fruit using explainable deep anomaly detection on X-ray images. Comput. Electron Agric. 197, 106962 https://doi.org/10.1016/j.compag.2022.106962.

Van De Looverbosch, T., Rahman Bhuiyan, Md.H., Verboven, P., Dierick, M., Van Loo, D., De Beenbouwer, J., Sijbers, J., Nicolaï, B., 2020. Nondestructive internal quality inspection of pear fruit by X-ray CT using machine learning. Food Control 113, 107170. https://doi.org/10.1016/j.foodcont.2020.107170.

Vaughn, K.C., Duke, S.O., 1984. Function of polyphenol oxidase in higher plants. Physiol. Plant 60, 106–112. https://doi.org/10.1111/j.1399-3054.1984.tb04258.x.

Weber, A., Thewes, F.R., Sellwig, M., Brackmann, A., Wünsche, J.N., Kittemann, D., Neuwald, D.A., 2019. Dynamic controlled atmosphere: Impact of elevated storage temperature on anaerobic metabolism and quality of 'Nicoter' apples. Food Chem. 298, 125017 https://doi.org/10.1016/j.foodchem.2019.125017.

Wood, R.M., Proske, M., de Freitas, S.T., Scheer, C., Vögele, R.T., Neuwald, D.A., 2022. Seasonal variation in calcium and ascorbic acid content at harvest related to internal browning in 'Braeburn' apple during controlled atmosphere storage. Sci. Hortic. 297, 110943 https://doi.org/10.1016/j.scienta.2022.110943.